Supplementary Information

Excitation dependence and independence of photoluminescence in carbon dots and graphene quantum dots: Insights into the mechanism of emission

Abu Bakar Siddique,[a] Syed Minhaz Hossain,[b] Ashit Kumar Pramanick,[c] and Mallar Ray[d, ‡,*]

[a.] *Aditya College of Engineering and Technology, Surampalem -533437, Andhra Pradesh, India.*

[b.] *Department of Physics, Indian Institute of Engineering Science and Technology, Shibpur, P.O.: Botanic Garden, Howrah: 711103, West Bengal, India*

[c.] *National Metallurgical Laboratory, Jamshedpur - 831007, Jharkhand, India*

[d.] *School of Engineering and Sciences, Tecnológico de Monterrey, Monterrey, 64849, Nuevo Leon, Mexico*

**E-mail: mallar.ray@tec.mx*

S1. Characterization details

Investigation of crystalline property of the synthesized nanostructures was carried out by x-ray diffraction (XRD) using a Brucker D8 advanced diffractometer operating at 40 kV, using Cu $K_{\alpha 1}$ (λ=1.54 Å) radiation. Bright field HR-TEM imaging and electron diffraction patterns were obtained by a JEOL-JEM, 2010 electron microscope operating at 200 kV. The samples were five times diluted and 2 µl of samples were deposited on carbon coated copper grids for HR-TEM measurements. We used a GATAN energy filtered TEM integrated with HR-TEM for EELS study of our samples. The transition of carbon was identified from the carbon-K ELNES spectrum and the low-loss EELS spectrum of the CDs was used to identify the surface plasmon and bulk plasmon peaks of the specimen sample. XPS measurements were conducted on an Omicron Multiprobe (Omicron NanoTechnology Gmbh, UK) spectrometer fitted with an EA125 (Omicron) hemispherical analyzer. Monochromatic Al-K_α source operated at 150 W was used and the pass energy of the analyzer was kept at 40 eV. A low-energy electron gun (SL1000, Omicron) with a large spot size was used for sample neutralization. The voltage of the electron gun was fixed at −3 V. UV-visible spectroscopy was performed using a JASCO V-750, UV-VIS spectrophotometer. Steady state PL property of different samples was investigated using a Horiba Jobin Yvon, Fluorolog-3 (Nanolog) spectrofluorometer (model FL3-11) fitted with a 450 W xenon lamp source, photomultiplier tube detector and single grating monochromator. During observation, entry and exit slit widths were kept at 1 nm

(bandpass units) and the integrating time was 1s. Absolute PL QY of the samples were estimated by recording the PL spectra using an integrating sphere following the method proposed by Suzuki et al.[1] Fluorescence decay time was recorded using a Horiba, Fluorolog-3 modular multifunctional time correlated single photon counting (TCSPC) lifetime spectrofluorometer.

S2. X-ray diffraction of 0D carbon system

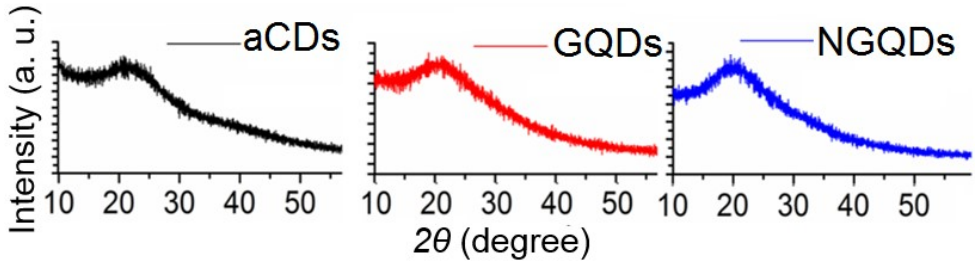

Figure S1: XRD profile of the aCD, GQD and NGQD powders.

XRD patterns of all the synthesised 0D carbon powders — aCDs, GQDs and NGQDs, exhibit broad diffraction peaks centred around $\sim 2\theta = 22^\circ$ and appear to be all identical as shown in Figure S1. The powder XRDs are therefore rather useless in identifying the samples and their differences. Nevertheless, the broad hump in aCDs confirm about the carbonisation of glucose via ultrasonic treatment at room temperature. Such a hump has been widely observed in XRD patterns of amorphous carbon.[2] Similarly, the humps observed in GQD and NGQD patterns confirm the carbonisation of citric acid via hydrothermal treatment at high temperature. A peak at $2\theta \sim 25^o$ is expected for the GQDs corresponding to diffraction from planes having *d*-spacing values of 0.35 nm. Typically, this distance is the π-stacking distance of the π-stacked graphene rings in the presence of a layered graphene structure of the GQDs prepared by hydrothermal process[3-5] Although we do not see any sharp peak we do observe that the broad hump peaks in the same region. The broad diffraction peaks are due to the small size and disordered cluster of carbon atoms. Similar patterns have been widely observed in XRD patterns of crystalline CDs or GQDs.[4, 5] The aCDs have a marginally broader hump compared to GQDs and NGQDs due to its amorphous arrangement, which confirmed by the absence of any fringes in the high magnification image of HR-TEM, or by the absence of any spot or ring in the SAEDP of aCDs.

S3. X-ray photoelectron spectroscopy of 0D carbon system

X-ray photoelectron spectroscopy (XPS) measurements were carried out to investigate the composition and surface groups of the carbon nanostructures. Two strong peaks at 285.5 eV and 532.5 eV are detected in the wide-scan XPS spectrum of aCD (Figure S2a) which are due

to carbon and oxygen, respectively.[6] The de-convoluted C1s spectrum of aCDs shown in Figure S2b, has four components, corresponding to C=C (sp^2 carbon) at 283.2 eV, C-C (sp^3 carbon) at 284.7 eV, C-OR and COOR at 285.4 eV and 289.5 eV, respectively. The measured O1s spectrum (Figure S2c) can be de-convoluted to three components peaking at 529.6, 531.1 and 532 eV, which are due to the C=O, C-OH and C-O-C groups, respectively.[7, 8] The XPS data confirms the presence of both sp^2 and sp^3 along with other expected compounds of C, H and O.

The wide-scan XPS spectrum of GQDs also has two strong peaks at 285 eV and 532.5eV related to carbon and oxygen (Figure S2d). Here too, the de-convoluted C1s spectrum (Figure S2e) has four components, corresponding to C=C (sp^2 carbon) at 284.5 eV, C-C (sp^3 carbon) at 285.8 eV, C=O and COOH at 288.6 eV and 289.9 eV, respectively. The point to note here is the intense peak of sp^2 carbon and comparatively much weaker peak of sp^3 carbon suggesting the dominant formation of graphene. The measured O1s spectrum (Figure S2f) can be de-convoluted to two components peaking at 531.5 and 532.5 eV, which are due to the C-O and C=O groups, respectively.[8, 9]

As expected the wide-scan XPS spectrum of NGQDs shown in Figure S2g detected a strong nitrogen peak at 400 eV along with carbon and oxygen peaks at 285 eV, and 530 eV, respectively, indicating successful insertion of nitrogen in the graphitic structure.[10] The de-convoluted C1s spectrum (Figure S2h) has three components, corresponding to C=C (sp^2 carbon) at 284.5 eV, C-C (sp^3 carbon) at 285.8 eV and nitrous-carbon at 287.55 eV, respectively.[11] Like the GQDs, the NGQD sample shows a much weaker but resolvable peak due to sp^3 carbon implying that the NGQD are dominantly graphene-like. The N1s spectrum (Figure S2i) can also be de-convoluted to two components peaking at 399.25 and 400.25 eV, which are due to the aromatic-N and surface-NH_2 respectively.[12] The high-resolution spectrum of C1s and N1s clearly indicates the incorporation of nitrogen into the carbon backbone. The O1s spectrum (Figure S2j) can be de-convoluted to two components peaking at 531.1 and 532.2 eV, which are due to the C-O and C=O groups, respectively.[9] The presence of surface-NH_2 in the pronounced N1s peak ensures the surface passivation by the amines in the NGQDs, which is also confirmed by the presence of N-H bonding vibration observed in the FTIR spectrum (discussed in the Supplementary information, Figure S3). Since amino-groups are electron-donating, they enhance the conjugation degree of amine-passivated NGQDs.

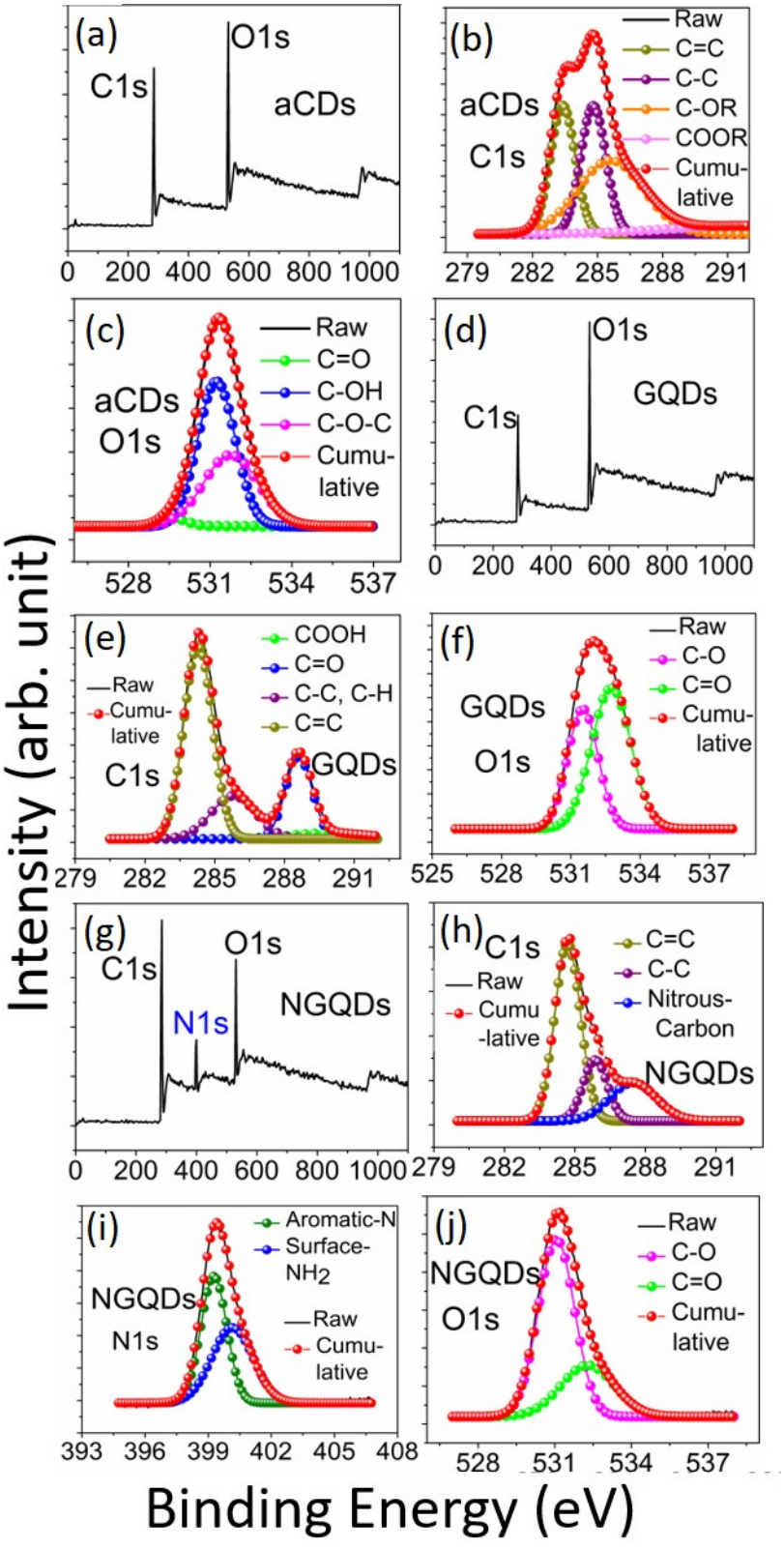

Figure S2: XPS spectra of the 0D carbon nanostructures. (a) Wide scan spectrum of the aCDs; De-convoluted (b) C1s, and (c) O1s spectra, of the aCDs; (d) Wide scan spectrum of the GQDs; De-convoluted of XPS spectra (e) C1s; and (f) O1s of the GQDs. (f) Wide scan spectrum of the NGQDs; de-convoluted (h) C1s spectra, (i) N1s spectra, and (j) O1s spectra of the NGQDs

S4. FTIR study of 0D carbon system

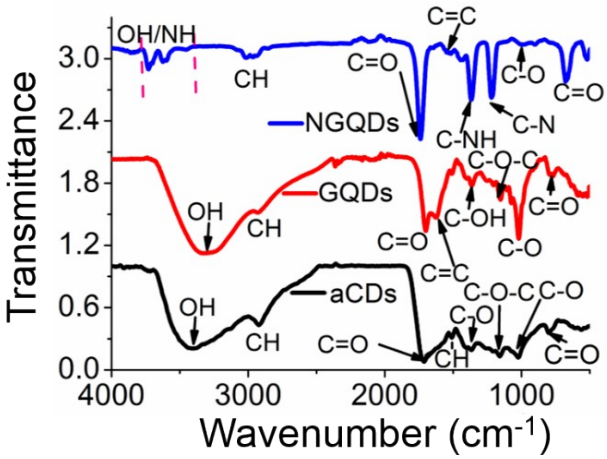

Figure S3: FTIR spectra of aCDs, GQDs and NGQDs

The three FTIR spectra shown in Figure S3, corresponding to the three samples, display several peaks related to the chemical bonds present in 0D carbon systems. The FTIR spectrum of aCDs reveal an absorption band spanning from 3640 to 3160 cm^{-1} which correspond to stretching vibrations of the OH bond.[13] The presence of such bonds is possibly responsible for imparting hydrophilicity and consequent water dispersibility of the CDs. The bands peaking at 1760 cm^{-1} and 1150 cm^{-1} may be assigned to the stretching vibrations of C=O and C-O, respectively,[3] suggesting that the surface of carbon clusters are passivated by oxygen containing surface groups that are spontaneously derived out of the carbonization process of dextrose. FTIR spectrum of GQDs exhibits characteristic similar to aCDs, since both are self-passivated by oxygen containing functional groups. The spectrum of pristine GQD demonstrates the presence of oxygen: C–O (1097 cm^{-1}), C–OH (1384 cm^{-1}), C=O in carboxylic acid and carbonyl moieties (1635 and 1726 cm^{-1}, respectively), and O-H (~3410 cm^{-1}).[14] For the NGQDs, FTIR spectrum shown in Figure S3, the bands peaking at 3300–3600 cm^{-1} is for the in-plane stretching vibrations of N–H along with the O-H stretching vibrations. The peaks at 1730 cm^{-1} and 1560 cm^{-1} are due to stretching vibrations from C=O,[15] and C=C, respectively, which are usually observed in reduced graphene oxide aromatic rings[14] This also confirms about the crystallinity of NGQDs. The peak at 1376 cm^{-1} is from the bending vibration of C-NH,[16] and the peaks at 1100–1260 cm^{-1} are due to OH deformation and C-N stretching vibrations.[17] This clearly indicates the successful incorporation of nitrogen atoms into the GQDs leading to the formation of NGQDs. Both GQDs and NGQDs exhibit the peaks corresponding to the C=C, indicating the formation of π-π conjugation in the structures.

S5. Graphical review: The graphical review of emission peak positions for different excitation wavelengths, as reported in significant published works.

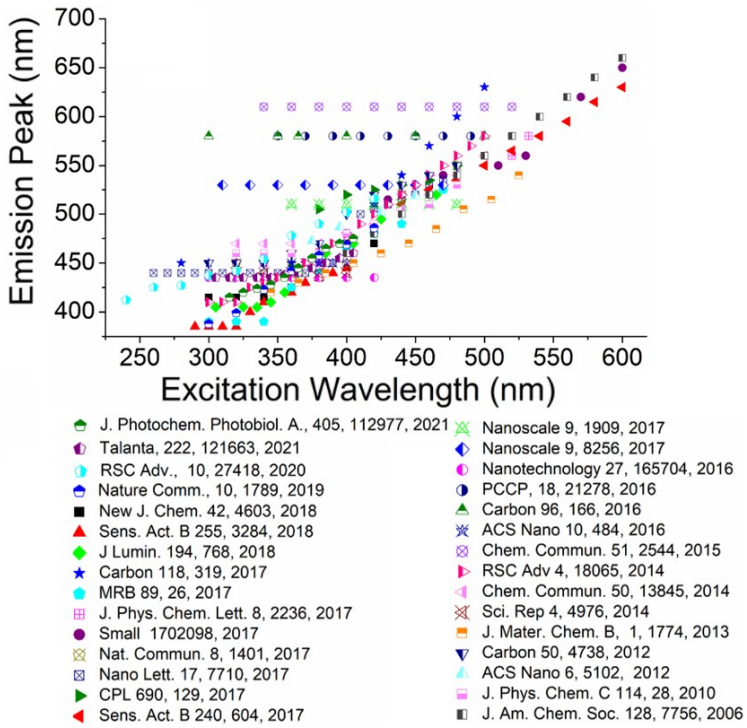

Figure S4: Variation of emission peak position with excitation wavelength for (different variants of 0D carbon studied and reported in literature.

S6. Temperature dependent PL: Temperature dependent PL studies provide important insights into emission mechanism. We recorded the emission spectra corresponding to different excitation energies for all the 0D systems for temperature varying from 30^0C to 70^0C. The temperature dependence of fluorescence spectra are shown in Figures S4 a-d. The PL peak position corresponding to a particular excitation energy remains invariant under change of temperature. The intensity of emission, however, consistently decreases almost linearly with increase in temperature for all the cases as shown in Figure S4 d. These temperature dependent monotonous decrease of PL intensity has been observed previously by other groups.[18-20] The reasons for decrease in the intensity with the temperature could be due to several relaxation processes like, Auger nonradiative scattering and thermally activated trapping in surface and/or defect states.[20] Non-radiative relaxation due to the thermal processes are most likely the contributing factor for such temperature dependent behaviour in 0D nanostructures.[21-24] In our study we have controlled to low excitations density by controlling the slits width, so Auger scattering may be ruled out. Therefore, phonon assisted nonradiative relaxations within a band or at the surface/interface states should be the dominant process responsible for decrease in the

intensity. The monotonous linear decrease in the PL intensity with rise in temperature also support non-radiative losses.

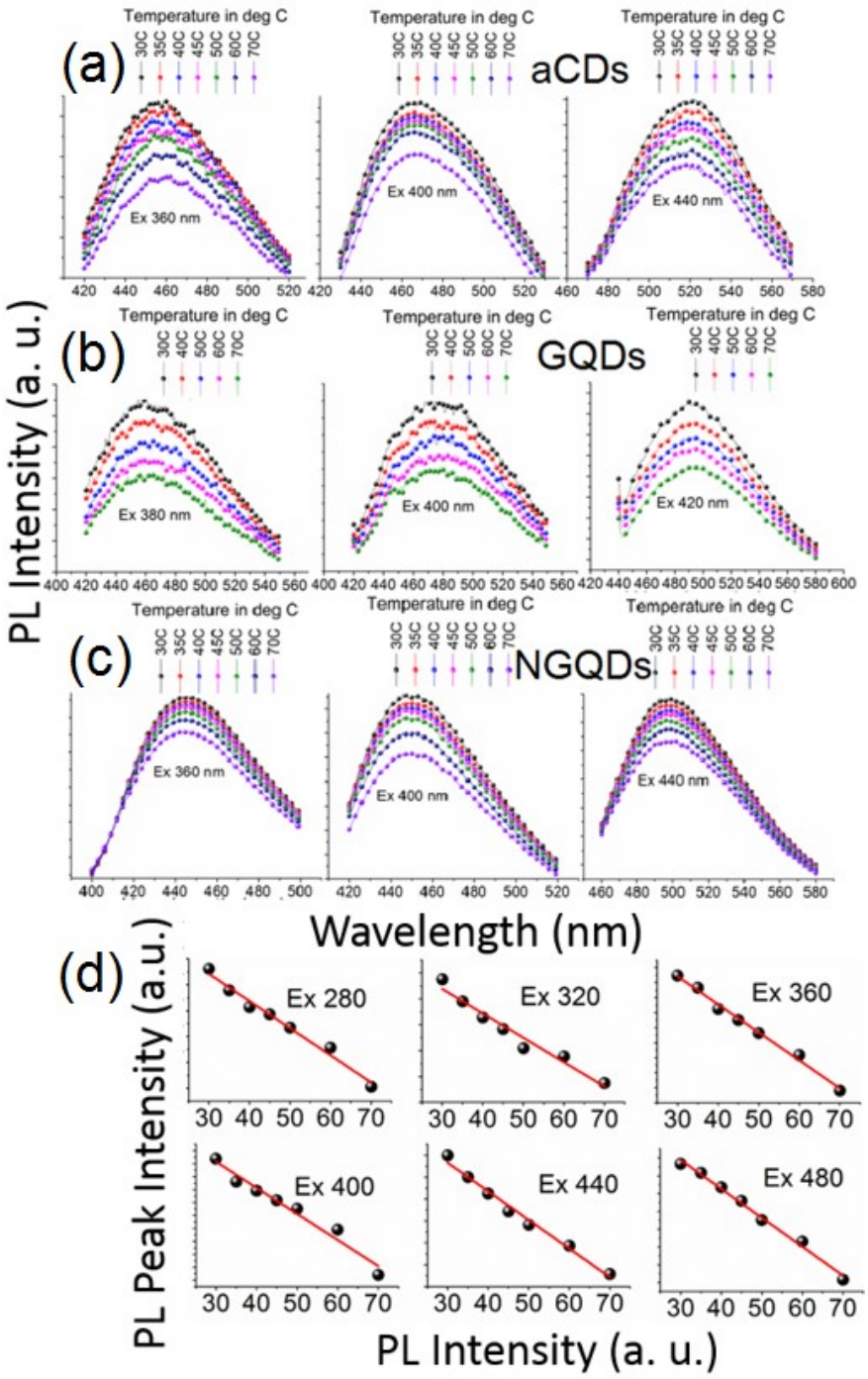

Figure S5: Temperature dependent PL emission spectra of CDs at different excitations: (a) aCD; (b) GQDs and (c) NGQDs; and (d) linear decrease of intensity of PL peak with temperature for the GQDs recorded at different excitation energies.

The PL quantum yield (QY_{PL}) depends on both radiative decay and nonradiative decay of excited states, that can be related as: $QY_{PL} = {k_r}/{k_r + k_{nr}}$, where k_r is radiative decay rate and k_{nr} is non-radiative decay rate. In general, radiative relaxation is not affected by temperature so the radiative decay rate is not affected. Whereas, non-radiative decay rate is dependent on temperature by Boltzmann law, given by: $Aexp^{\frac{-E}{kT}}$, where A is a constant, E is energy of state, k is the Boltzmann's constant and T is the temperature. As the temperature increases, the non-radiative decay rate increases, hence QY_{PL} also decreases. We are also aware that: $I_{PL} = QY_{PL} * A_{PL,}$ Where, I_{PL} is PL intensity, QY_{PL} is the PL quantum yield and A_{PL} is the PL absorption. So, intensity of the PL decreases linearly with the rise in temperature due to non-radiative losses.[19]

S7. PL decay dynamics:

The average fluorescence lifetime was calculated from the equation (1) as proposed by Sillen et al. and Joseph R. Lakowicz in " Principles of fluorescence spectroscopy." .[25, 26]

$$<\tau>=\frac{\sum_{i=1}^{n}\alpha_i\tau_i^2}{\sum_{i=1}^{n}\alpha_i\tau_i} \qquad (1)$$

where τ_i are the fluorescence decay times, α_i are the normalized pre-exponential values and n is the total number of decay components.

The radiative rate constant (k_r) and the nonradiative rate constant (k_{nr}) were estimated by using the following equations (2) and (3) respectively.[27]

$$QY = k_r * \tau_{avg} \qquad (2)$$

$$k_r + k_{nr} = 1/\tau_{avg} \qquad (3)$$

where, QY is the photoluminescence quantum yield of the CDs

Table S1: Parameters estimated from the PL decay

Samples	τ_1 (ns)	τ_2 (ns)	τ_3 (ns)	τ_{avg} (ns)	k_r (ns^{-1})	k_{nr} (ns^{-1})

aCDs	2.3168	0.375935	6.484977	2.90440208	0.134278929	0.210026017
GQDs	0.495955	2.547455	8.211507	3.20385632	0.015606193	0.296517666
NGQDs	2.479985	14.95321	-	14.3635851	0.044557121	0.025063381

References

1. K. Suzuki, A. Kobayashi, S. Kaneko, K. Takehira, T. Yoshihara, H. Ishida, Y. Shiina, S. Oishi and S. Tobita, *Physical Chemistry Chemical Physics*, 2009, **11**, 9850-9860.
2. X. Li, S. Zhang, S. A. Kulinich, Y. Liu and H. Zeng, *Scientific reports*, 2014, **4**, 4976.
3. S. Sahu, B. Behera, T. K. Maiti and S. Mohapatra, *Chemical Communications*, 2012, **48**, 8835-8837.
4. X. Wu, F. Tian, W. Wang, J. Chen, M. Wu and J. X. Zhao, *Journal of Materials Chemistry C*, 2013, **1**, 4676-4684.
5. Z. L. Wu, M. X. Gao, T. T. Wang, X. Y. Wan, L. L. Zheng and C. Z. Huang, *Nanoscale*, 2014, **6**, 3868-3874.
6. Z. Yang, M. Xu, Y. Liu, F. He, F. Gao, Y. Su, H. Wei and Y. Zhang, *Nanoscale*, 2014, **6**, 1890-1895.
7. W. Chen, C. Hu, Y. Yang, J. Cui and Y. Liu, *Materials*, 2016, **9**, 184.
8. J. Wei, J. Shen, X. Zhang, S. Guo, J. Pan, X. Hou, H. Zhang, L. Wang and B. Feng, *RSC Advances*, 2013, **3**, 13119-13122.
9. L. Tang, R. Ji, X. Cao, J. Lin, H. Jiang, X. Li, K. S. Teng, C. M. Luk, S. Zeng and J. Hao, *ACS nano*, 2012, **6**, 5102-5110.
10. D. Qu, M. Zheng, L. Zhang, H. Zhao, Z. Xie, X. Jing, R. E. Haddad, H. Fan and Z. Sun, *Scientific reports*, 2014, **4**, 5294.
11. L.-J. Bian, F. Luan, S.-S. Liu and X.-X. Liu, *Electrochimica Acta*, 2012, **64**, 17-22.
12. Y. Yang, J. Cui, M. Zheng, C. Hu, S. Tan, Y. Xiao, Q. Yang and Y. Liu, *Chemical Communications*, 2012, **48**, 380-382.
13. L. Zhao, F. Di, D. Wang, L.-H. Guo, Y. Yang, B. Wan and H. Zhang, *Nanoscale*, 2013, **5**, 2655-2658.
14. V. Ţucureanu, A. Matei and A. M. Avram, *Critical reviews in analytical chemistry*, 2016, **46**, 502-520.

15. H. Tetsuka, A. Nagoya, T. Fukusumi and T. Matsui, *Advanced Materials*, 2016, **28**, 4632-4638.

16. H. Zhang, Y. Chen, M. Liang, L. Xu, S. Qi, H. Chen and X. Chen, *Analytical chemistry*, 2014, **86**, 9846-9852.

17. D. Qu, M. Zheng, P. Du, Y. Zhou, L. Zhang, D. Li, H. Tan, Z. Zhao, Z. Xie and Z. Sun, *Nanoscale*, 2013, **5**, 12272-12277.

18. C. Wang, Z. Xu, H. Cheng, H. Lin, M. G. Humphrey and C. Zhang, *Carbon*, 2015, **82**, 87-95.

19. C. Li and Y. Yue, *Nanotechnology*, 2014, **25**, 435703.

20. P. Yu, X. Wen, Y.-R. Toh and J. Tang, *The Journal of Physical Chemistry C*, 2012, **116**, 25552-25557.

21. D. Valerini, A. Creti, M. Lomascolo, L. Manna, R. Cingolani and M. Anni, *Physical Review B*, 2005, **71**, 235409.

22. X. Wen, J. A. Davis, L. Van Dao, P. Hannaford, V. A. Coleman, H. Tan, C. Jagadish, K. Koike, S. Sasa and M. Inoue, *Applied physics letters*, 2007, **90**, 221914.

23. A. Al Salman, A. Tortschanoff, M. Mohamed, D. Tonti, F. Van Mourik and M. Chergui, *Applied Physics Letters*, 2007, **90**, 093104.

24. X. Wen, A. Sitt, P. Yu, Y.-R. Toh and J. Tang, *Physical Chemistry Chemical Physics*, 2012, **14**, 3505-3512.

25. A. Sillen and Y. Engelborghs, *Photochemistry and photobiology*, 1998, **67**, 475-486.

26. C. Albrecht, *Analytical and Bioanalytical chemistry*, 2008, **390**, 1223-1224.

27. J. R. Lakowicz, *Principles of fluorescence spectroscopy*, Springer Science & Business Media, 2013.